Temporal fluctuations in the bosonic Josephson junction as a probe for phase space tomography

Christine Khripkov[1], Doron Cohen[2], and Amichay Vardi[1]
Departments of [1] Chemistry and [2] Physics, Ben-Gurion University of the Negev, Beer-Sheva 84105, Israel

We study the long time coherence dynamics of a two-mode Bose-Hubbard model in the Josephson interaction regime, as a function of the relative phase and occupation imbalance of an arbitrary coherent preparation. We find that the variance of the long time fluctuations of the one-body coherence can be factorized as a product of the inverse participation number $1/M$ that depends only on the preparation, and a semi-classical function $C(E)$ that reflects the phase space characteristics of the pertinent observable. Temporal fluctuations can thus be used as a sensitive probe for phase space tomography of quantum many-body states.

The two mode Bose-Hubbard Hamiltonian (BHH) appears in different guises in a perplexing variety of fields. Cast in spin form, it is known in nuclear physics as the Lipkin-Meshkov-Glick (LMG) model of shape phase transitions [1]. It is broadly used to describe interacting spin systems [2] and serves as a paradigm for squeezing and entanglement [3]. As such, it offers schemes for the generation of squeezed states for optical interferometry below the standard quantum limit [4], and its matter-wave equivalent [5]. It is commonly employed to describe the Josephson dynamics in systems of bosonic atoms in double-well potentials [6] and suggests prospects for the generation of macroscopic superposition states [7]. The same model is also known in condensed matter physics as the integrable dimer model [8] with applications to the dynamics of small molecules, molecular crystals, and self-trapping in amorphous semiconductors.

Like the paradigmatic Jaynes-Cummings model in quantum optics [9], the bimodal BHH dynamics with a coherent spin state preparation exhibits a series of collapses and revivals of its single-particle coherence due to interactions [10–13]. These recurrences are manifested in the collapse and revival of the Rabi-Josephson population oscillations, or of the multi-realization fringe visibility, when the two condensates are released and allowed to interfere. Below we study the long time BHH dynamics for general coherent spin preparations $|\theta,\phi\rangle$. In such states all particles occupy a single superposition of the two modes, with a normalized population imbalance $S_z = \cos(\theta)$ and a relative phase ϕ.

The characteristics of this dephasing-rephasing dynamics strongly depend on the dimensionless interaction parameter $u = UN/K$, where U is the interaction strength, N is the total particle number, and K is the hopping amplitude. In the linear Rabi regime ($u < 1$) time evolution is straightforward because the interaction is not sufficiently strong to modify the one-body nature of the dynamics. Accordingly, one observes only coherent Rabi oscillations in the population difference with a typical frequency $\omega_J \equiv \sqrt{K(K-UN)} = K\sqrt{1-u} \approx K$ which reflects mainly the coupling K between the two modes, accompanied by a small modulation of the single-particle coherence at the same frequency.

The coherence dynamics in the strong interaction Fock regime ($u > N^2$) is also fairly simple because it reflects the Fock basis expansion of the initial coherent preparation. The expected coherence recurrences have been observed experimentally [14, 15] with a striking demonstration of exceptionally long time dynamics, allowing to probe effective multi-body interactions through the dependence of U on the number of atoms [16].

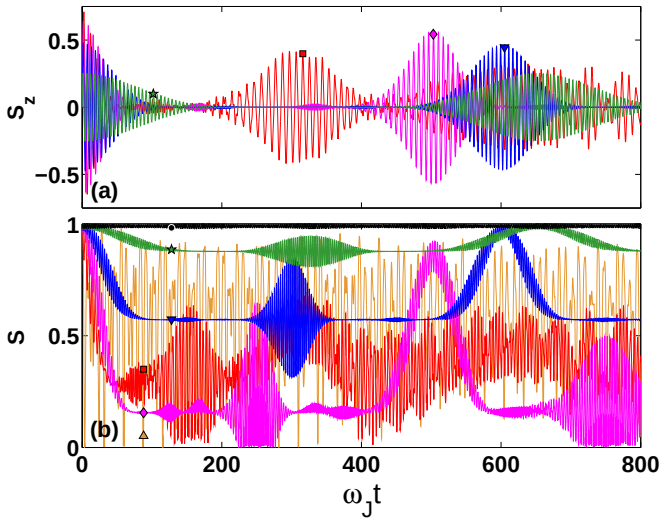

FIG. 1: (color online) Collapse and revival dynamics of the normalized population imbalance S_z (top) and of the single-particle coherence S (bottom) for representative equal-population coherent preparations $|\pi/2,\phi\rangle$, with $\phi = 0$ ($\circ$), 0.2π ($\star$), 0.4π ($\triangledown$), 0.6π ($\diamond$), 0.8π ($\square$), and π ($\triangle$). Note that in the last case $S_z(t) = 0$ at any moment, while $S(t)$ oscillates wildly. The BHH parameters here and in all subsequent figures are $N = 100$ and $u = 5$, corresponding to the Josephson regime.

The dynamics in the Josephson regime ($1 < u < N^2$) is by far richer and more intricate, reflecting the coexistence of three distinct phase space regions [11, 12]. Unlike the Fock-space recurrences which only depend on the population imbalance, the Josephson coherence dynamics is also highly sensitive to the relative phase. Previous work has considered specific preparations that were of contemporary experimental relevance, e.g. small perturbation of the ground state that results in Josephson oscillations, or

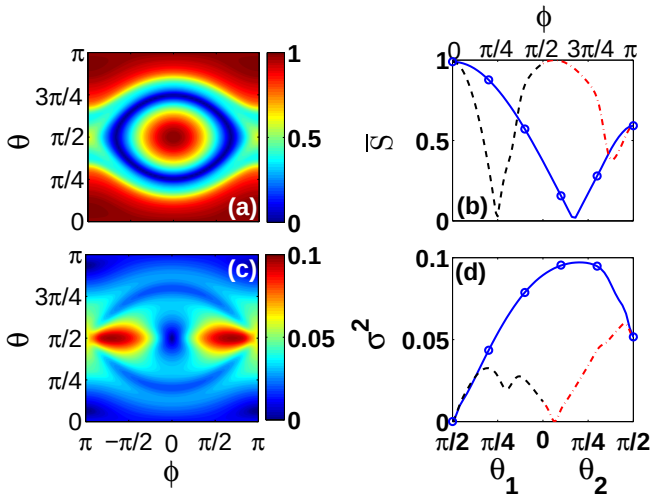

FIG. 2: (color online) Long time average (a,b) and variance (c,d) of the one-particle coherence $S(t)$, starting from the coherent preparation $|\theta,\phi\rangle$. Panels (b) and (d) show a section along the Equator $\theta=\pi/2$ with $\phi\in[0,\pi]$ (blue solid line), with appended sections along the arcs $\phi=0$ with $\theta_1\in[\pi/2,0]$ (black dashed line), and $\phi=\pi$ with $\theta_2\in[0,\pi/2]$ (red dashed line). Symbols correspond to values which were calculated from a direct numerical propagation of the states in Fig.1.

a large population imbalance that leads to self-trapping [17]. Here we adopt a global, tomographic approach by characterizing the long time temporal quantum fluctuations for *all* possible coherent preparations. This appears to be a formidable task, but as shown below, a relatively simple semi-classical perspective provides an adequate framework for the required analysis.

Observations.– The intricacy of the Josephson regime quantum dynamics is illustrated in Fig.1 and in Fig.2. Various coherent preparations lead to qualitatively different behavior, depending on the initial population imbalance $\cos\theta$ and on the relative phase ϕ. The cause of this diversity is that different coherent preparations sample different parts of the spectrum. Each coherent spin state constitutes a superposition of eigenstates that can be associated with qualitatively different regions in the corresponding classical phase space. This is in a stark contrast to the Rabi and Fock regimes, where the eigenstates occupy, so to say, a single component phase space that allows only one type of motion.

Our main finding below is related to a striking factorization in the calculation of the variance of the temporal fluctuations of the pertinent observables. Given an observable $\hat{A}$ with a fluctuating expectation value $A(t)=\langle\hat{A}\rangle_t$ that has long time average $\overline{A(t)}$, we find that its variance can be approximated quite accurately as a product of a quantum term and a semi-classical term:

$$\sigma_A^2 \equiv \overline{A^2(t)}-\overline{A(t)}^2 = \frac{1}{M}C_A(E). \qquad (1)$$

Here M is the participation number which depends only on the preparation, while $C_A(E)$ corresponds to the classical fluctuations of A along a mean-field trajectory that has an energy E. The implications of this observation for phase space tomography are further discussed in the concluding paragraph. We now turn to a detailed presentation of the analysis.

The BHH.– We consider a similar scenario to that in Ref. [15], which observed the long time collapse and revival of coherence in the Fock regime. For such strong interactions the modes are essentially decoupled, hence the dynamics is fully captured by the Gutzwiller ansatz of a direct product of single-site states, each of which is a coherent wavepacket of number states [14, 15, 18, 19]. Thus, in the Fock regime the two-mode BHH generates precisely the same coherence dynamics as the many-site BHH of a BEC in an optical lattice. This allows for monitoring the fringe visibility in single shot interferometery of an optical lattice, rather than repeating a two-mode experiment many times [14, 15, 19]. In the Josephson regime, the dynamics of a lattice with one mode per site is quite different from the two-mode dynamics. However, the two-mode model can be realized with two spin components in each isolated site [20] or with an array of independent double wells [21], thus retaining the convenience of single-shot measurements.

Assuming that no bias field is applied, the pertinent BHH is,

$$\begin{aligned}\mathcal{H} &= -K\left(\hat{a}_1^\dagger\hat{a}_2+\hat{a}_2^\dagger\hat{a}_1\right)\\ &\quad+\frac{U}{2}\left[\hat{n}_1\left(\hat{n}_1-1\right)+\hat{n}_2\left(\hat{n}_2-1\right)\right], \qquad (2)\end{aligned}$$

where $\hat{a}_i$ and $\hat{a}_i^\dagger$ are bosonic annihilation and creation operators, respectively. The particle number operator in mode i is $\hat{n}_i=\hat{a}_i^\dagger\hat{a}_i$. Since the total particle number $\hat{n}_1+\hat{n}_2=N$ is conserved, we can eliminate respective c-number terms and obtain the BHH in spin form,

$$\hat{H} = -K\hat{J}_x+\ U\hat{J}_z^2\ , \qquad (3)$$

where $\hat{J}_x=(\hat{a}_1^\dagger\hat{a}_2+\hat{a}_2^\dagger\hat{a}_1)/2$, $\hat{J}_y=(\hat{a}_1^\dagger\hat{a}_2-\hat{a}_2^\dagger\hat{a}_1)/(2i)$, and $\hat{J}_z=(\hat{n}_1-\hat{n}_2)/2$. The number conservation becomes angular momentum conservation with $j=N/2$. Below we assume for simplicity that the interaction is repulsive $U>0$, but the $U<0$ case amounts to a simple transformation $K\mapsto-K$, and $E\mapsto-E$. Thus the phase space with attractive interaction is simply an inverted mirror image of the repulsive-inetraction case and there is no loss of generality. In this spin representation, each state is characterized by the normalized Bloch vector $\mathbf{S}\equiv\langle\mathbf{J}\rangle/j$, where its z projection $S_z=\cos(\theta)$ corresponds to the normalized population imbalance, its azimuthal angle ϕ corresponds to the relative phase between the modes, and its length S corresponds to the single-particle coherence.

The phase space structure of the BHH is set by the previously defined dimensionless interaction parameter u. Its characteristics in the three interaction regimes are discussed in great detail elsewhere [6, 11, 12]. Briefly, in the Josephson regime ($1<u<N^2$) the phase space contains two 'islands' that are separated from a 'sea' region

by a separatrix. The sea trajectories correspond to Rabi-Josephson population oscillations, whereas the island trajectories correspond to self-trapped phase-oscillations [17]. In the Fock regime ($u > N^2$) the sea becomes too small to support quantum states, while in the opposite limit - in the Rabi regime ($u < 1$) - the islands disappear, so that only Rabi-type oscillations are feasible.

Evolution.– We study the dynamics induced by the Hamiltonian of Eq.(2), or equivalently by Eq.(3), starting from an arbitrary spin coherent state preparation,

$$|\theta,\phi\rangle \equiv \frac{1}{N!}\left[\cos(\theta/2)\hat{a}_1^\dagger + \sin(\theta/2)e^{i\phi}\hat{a}_2^\dagger\right]^N |\text{vac}\rangle = \exp(-i\phi\hat{J}_z)\exp(-i\theta\hat{J}_y)\exp(i\phi\hat{J}_z)|j,-j\rangle, \quad (4)$$

where $|\text{vac}\rangle$ and $|j,-j\rangle$ are the vacuum states of the Heisenberg-Weil and SU(2) algebras, respectively. We focus our attention on experimentally relevant observables such as the population imbalance S_z and the single-particle coherence S. Note that S is the best fringe visibility one may expect to measure by proper manipulation of the Bloch vector, i.e. if we are allowed to perform any SU(2) rotation. The expected fringe visibility if interferometry is carried out without further manipulation is $g_{12}^{(1)} = (1/j)[|\hat{J}_x|^2 + |\hat{J}_y|^2]^{1/2}$. For presentation purpose we focus on S, but the results for $g_{12}^{(1)}$ are very similar.

The evolution of the population imbalance and of the one-particle coherence for several representative coherent preparations is shown in Fig.1. For each preparation $|\theta,\phi\rangle$ we obtain the long time-average and the variance of $S_z(t)$ and $S(t)$. These numerical-propagation values for the preparations of Fig.1 are represented by the symbols in Fig.2(b)(d). In order to see the overall picture, we plot in Fig.2(a)(c) an image of $\overline{S}(\theta,\phi)$ and $\sigma_S(\theta,\phi)$ for all the possible coherent preparations. We note parenthetically that in practice, the exact values are not obtained from finite time simulations, but deduced from the energy expansion as detailed in the analysis section below. As is exemplified in Fig. 2(b)(d), the agreement between the energy expansion (lines) and the numerical propagation (symbols) clearly validates the pertinent expressions.

Analysis.– In order to deduce the exact time average of any $A(t)$, we expand it in the energy basis as

$$A(t) = \sum_{\nu,\mu} c_\nu^* c_\mu A_{\nu\mu} \exp[(E_\nu - E_\mu)t/\hbar], \quad (5)$$

where $|E_\nu\rangle$ are the BHH eigenstates, $c_\nu = \langle E_\nu|\psi\rangle$ are the expansion coefficients of the initial state $|\psi\rangle = |\theta,\phi\rangle$, and $A_{\nu\mu} = \langle E_\nu|\hat{A}|E_\mu\rangle$. The long-time average eliminates the oscillating terms, hence $\overline{A(t)} = \sum_\nu p_\nu A_{\nu\nu}$, with probabilities $p_\nu \equiv |c_\nu|^2$, while the variance is

$$\sigma_A^2 = \sum_{\nu\neq\mu} p_\nu p_\mu |A_{\nu\mu}|^2 \ . \quad (6)$$

The matrix elements in Eq.(6) can be evaluated semiclassically using the following prescription [12, 22]: a classical trajectory of energy E is generated using the BHH mean field equations of motion, and $A_{cl}(t)$ is calculated; then the classical power-spectrum $\tilde{C}_A^{cl}(\omega)$ is obtained via a Fourier transform of $[A_{cl}(t) - \overline{A_{cl}}]$; and finally the result is divided by the mean level spacing ϱ at that energy, providing the approximation $|A_{\nu\mu}|^2 \approx \tilde{C}_A^{cl}(E_\nu - E_\mu)/(2\pi\varrho)$. This is a very general procedure which is usually applied to chaotic systems, but it applies equally well to the integrable non-linear motion of the two-mode BHH. Since the motion is periodic but highly non-linear, the integral over $C_A^{cl}(\omega)$ turns out to be the variance of a periodic function that contains many harmonics. One may say that the power spectrum of $A(t)$, though quantized, is semiclassically narrow but quantum-mechanically broad. The number of participating eigenstates that contribute to Eq.(6), is conventionally evaluated as $M \equiv [\sum_\nu p_\nu^2]^{-1}$. Assuming $M \gg 1$, approximating $p_\nu \approx 1/M$, and neglecting non-participating eigenstates, one obtains Eq.(1) where,

$$C_A(E) = \sum_{|r|>0} |A_{\nu\mu}|^2 = \int \tilde{C}_A^{cl}(\omega)\frac{d\omega}{2\pi}. \quad (7)$$

Above $r = (\nu - \mu)$ is the diagonal coordinate of the matrix, and it is implicit that the summation is carried out over a section $\nu + \mu = \text{const}$ such that $(E_\nu + E_\mu)/2 \sim E$.

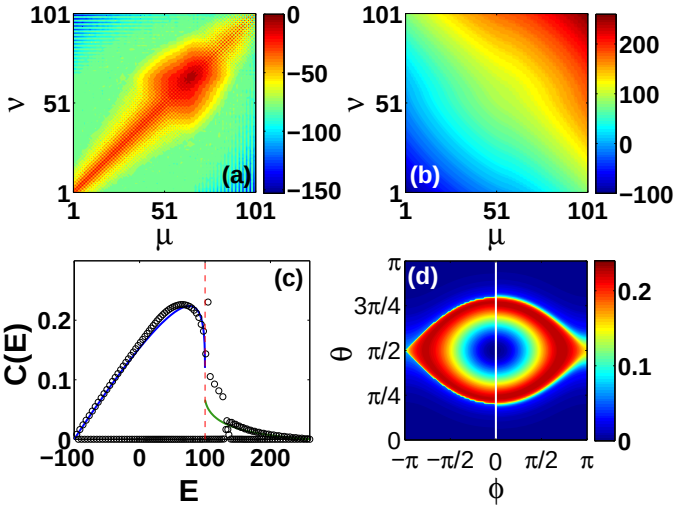

FIG. 3: (color online) Calculation of $C(E)$ for the observable $A = \hat{J}_z$. Panel (a) is an image of the matrix elements $|A_{nm}|$, with color-scale in log10 units. Panel (b) displays equal energy contours $E = (E_n + E_m)/2$. In panel (c) the function $C_A(E)$ is evaluated according to the middle (symbols) and the r.h.s. (lines) of Eq.(7). The dashed vertical line marks the separatrix energy $E = NK/2$. Panel (d) is a phase space image of $C_A(E)$. The left half of the image corresponds to the lines of panel (c), whereas the right side corresponds to the symbols.

Numerical verification.– In Fig. 3 we illustrate a representative evaluation of $C_A(E)$ for the population imbalance $A = J_z$. The matrix elements $(J_z)_{\nu\mu}$ are shown in panel Fig.3(a), confirming the assumptions of a

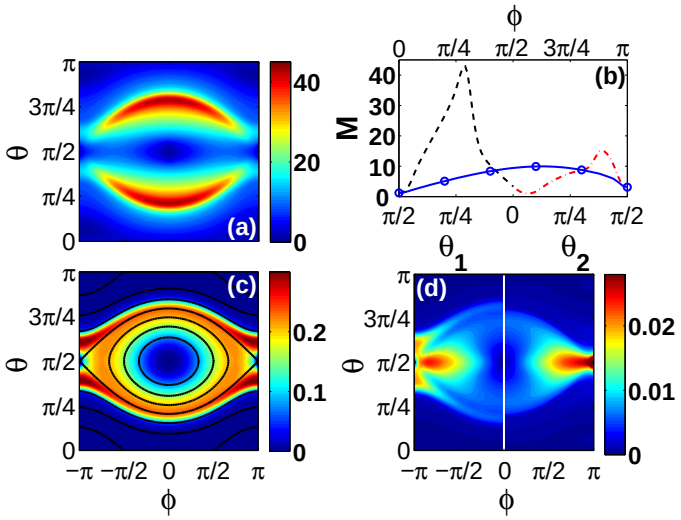

FIG. 4: (color online) The participation number of the coherent state preparations, and the long time fluctuations of the observable $A = \hat{J}_z$. Panel (a) displays the participation number $M(\theta, \phi)$ of the states $|\theta, \phi\rangle$. Panel (b) provides a cross-section of $M(\theta, \phi)$ along the same contour that has been defined in Fig. 2. Panel (c) overlays $M(\theta, \phi)\sigma_A^2(\theta, \phi)$ with the constant energy contours in phase space. Panel (d) displays the variance σ_A^2 as calculated from the approximation Eq. (1) (right half of the panel), compared with the actual value Eq.(6) (left half of the panel).

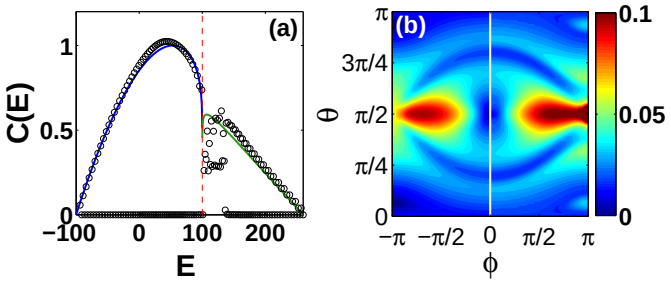

FIG. 5: (color online) Power spectrum $C_S(E)$ (a) and variance of fluctuations σ_S^2 (b) for the single-particle coherence S. Notations are the same as in Fig.3(c) and Fig.4(d). Note that the left half of the image is the same as Fig.2(c).

semiclassically narrow but quantum-mechanically broad spectrum. The equal energy contours in panel Fig.3(b) demonstrate that due to the semiclassical narrowness we can approximate the energy shell average by a summation over the diagonals $\nu + \mu = const$. The results of the summation over the matrix elements and the integration over the classical fluctuations according to Eq. (7) are compared in panel Fig.3(c), and the final contour map of the power spectrum in the phase space is presented for both methods in panel Fig.3(d). This comparison demonstrates the validity of the semiclassical approximation of the matrix elements.

In order to evaluate the variance of the fluctuations, we need to calculate the participation number M for a general coherent preparation $|\theta, \pi\rangle$. The result is shown in Fig.4(a)(b). Due to the factorization Eq.(1), this function needs be calculated only once for all desired observables. While we do not have a closed analytic expression for $M(\theta, \phi)$, its characteristic value and its dependence on u and N in the different phase space regions can be evaluated from general considerations as detailed in Ref. [12]. Generally speaking, the highest participation numbers are obtained at the top of the separatrix and scale as $M \approx \sqrt{N}\log(N/u)$, i.e. like the square root of N. By contrast, the equatorial states $|\pi/2, 0\rangle$ and $|\pi/2, \pi\rangle$ have participation numbers of order unity: $M(\pi/2, 0) \approx \sqrt{u}$ and $M \approx \sqrt{u}\log(N/u)$, respectively.

Fig.4(c) confirms our result that the long time temporal fluctuations can be factorized as the ratio of the power-spectrum and the participation number. Indeed, when we plot $M\sigma_A^2$ as a function of θ and ϕ we obtain that the $M\sigma_A^2 = \text{const}$ contours coincide with the constant-energy lines. Thus, $M\sigma_A^2$ is only a function of E. The only exception is in the immediate vicinity of the coherent state $|\pi/2, \pi\rangle$ for which the semi-classical assumption $M \gg 1$ does not hold.

Having ascertained the semiclassical factorization, it remains to verify the quantitative agreement between the values of the contour lines of $M\sigma_A^2$ and the semiclassically calculated $C_A(E)$. In Fig.4(d) we use the participation number M and the calculated $C_{J_z}(E)$ to predict the variance of the population imbalance oscillations for the various preparations, and compare it to the results obtained by a numerical propagation, or by using Eq.(6). The agreement is good, confirming the validity of Eq.(1) and demonstrating that the long time population oscillations will only survive in the vicinity of the unstable equal-population $\phi = \pi$ preparation, where the power spectrum is large and the participation number is small. Note that the classical fluctuations are large for the other separatrix preparations, too, but away from $\phi = \pi$ the participation number is large, and hence the quantum fluctuations are quenched. Similar results are shown in Fig.5 for the variance of the coherence fluctuations.

Summary.– The magnitude of the long-time quantum fluctuations of an arbitrary observable A can be deduced from the tractable classical dynamics and from the a-priori known participation number of all coherent preparations. Moreover, because $C_A(E)$ only depends on energy, it is possible to obtain a tomographic image of the phase space from the observed fluctuations by plotting $M\sigma_A^2$. The contours of this plot trace the equal energy lines and their values are specific to the measured observable. Eq. (1) constitutes a dramatic reduction in complexity and offers great insight on the dynamics of the two-mode BHH. It is successfully employed above to characterize the observed fluctuations in population imbalance, one-particle coherence, and fringe-visibility. In a larger context, these findings are related to studies of thermalization in isolated many-body quantum systems

[23].

Acknowledgments.– This research was supported by the Israel Science Foundation (grant Nos. 346/11 and 29/11) and by the United States-Israel Binational Science Foundation (BSF).

[1] H. J. Lipkin, N. Meshkov, and A. J. Glick, Nucl. Phys. **62**, 188 (1965); P. Ribeiro, J. Vidal, and R. Mosseri, Phys. Rev. Lett. **99**, 050402 (2007); P. Ribeiro, J. Vidal, and R. Mosseri, Phys. Rev. E **78**, 021106 (2008).
[2] R. Botet and R. Julien, Phys. Rev. B **28**, 3955 (1983).
[3] M. Kitagawa and M. Ueda, Phys. Rev. A **47**, 5138 (1993); A. Sorensen and K. Molmer, Phys. Rev. Lett. **86**, 4431 (2001); A. Sorensen, L. M. Duan, J. I. Cirac, and P. Zoller, Nature **409**, 63 (2001); A. Micheli, D. Jaksch, J. I. Cirac, and P. Zoller, Phys. Rev. A **67**, 013607(2003); C. Bodet, J. Esteve, M. K. Oberthaler, and T. Gasenzer, Phys. Rev. A **81**, 063605 (2010).
[4] C. M. Caves, Phys. Rev. D **23**, 1693 (1981); B. Yurke, S. L. McCall, and J. R. Klauder, Phys. Rev. A **33**, 4033 (1986); M. J. Holland and K. Burnett, Phys. Rev. Lett. **71**, 1355 (1993);
[5] C. Gross, T. Zibold, E. Nicklas, J. Esteve, and M. K. Oberthaler, Nature **464**, 7292 (2010); M. F. Riedel, P. Böhi, Y. Li, T. W. Hänsch, A. Sinatra, and P. Treutlein, Nature bf 464, 1170 (2010).
[6] A. V. Turbiner, Commn. Math. Phys. **118**, 467 (1988); V. V. Ulyanov and O. B. Zaslavskii, Phys. Rep. **216**, 179 (1992); A. Vardi and J. R. Anglin, Phys. Rev. Lett. **86**, 568 (2001); J. R. Anglin and A. Vardi, Phys. Rev. A **64**, 013605 (2001); M. Albiez *et al.*, Phys. Rev. Lett. **95**, 010402 (2005); R. Gati and M. Oberthaler, J. Phys. B **40**, R61 (2007);
[7] J. I. Cirac, M. Lewenstein, K. Molmer, and P. Zoller, Phys. Rev. A. **57**, 1208 (1998); T.-L Ho and C. V. Ciobanu, J. Low Temp. Phys. **135**, 257 (2004); Y. P. Huang and M. G. Moore, Phys. Rev. A. **73**, 023606 (2006).
[8] J. C. Eilbeck, P. S. Lomdahl, and A. C. Scott, Physica 16D, 318 (1985); L. Bernstein, J. C. Eilbeck, and A. C. Scott, Nonlinearity **3**, 293 (1990); S. Aubry, S. Flach, K. Klado, and E. Olbrich, Phys. Rev. Lett. **76**, 1607 (1996); G. Kalosakas and A. R. Bishop, Phys. Rev. A **65**, 043616 (2002).
[9] E.T. Jaynes, F.W. Cummings, Proc. IEEE **51**, 89 (1963); F.W. Cummings, Phys. Rev. **140**, A1051 (1965); J.H. Eberly, N.B. Narozhny, and J.J. Sanchez-Mondragon, Phys. Rev. Lett. **44**, 1323 (1980).
[10] G. J. Milburn, J. Corney, E. M. Wright, and D. F. Walls, Phys. Rev. A **55**, 4318 (1997); A. Imamoglu, M. Lewenstein, and L. You, Phys. Rev. Lett. **78**, 2511 (1997); G. Kalosakas, A. R. Bishop, and V. M. Kenkre, Phys. Rev. A **68**, 023602 (2003); K. Pawlowski, P. Zin, K. Rzazewski, and M. Trippenbach, Phys. Rev. A **83**, 033606 (2011).
[11] E. Boukobza, M. Chuchem, D. Cohen, and A. Vardi, Phys. Rev. Lett. **102**, 180403 (2009).
[12] M. Chuchem, K. Smith-Mannschott, M. Hiller, T. Kottos, A. Vardi, and D. Cohen, Phys. Rev. A **82**, 053617(2010).
[13] M. Egorov *et al.*, Phys. Rev. A **84**, 21605(R) (2011).
[14] M. Greiner, M. O. Mandel, T. Hänsch, and I. Bloch Nature **419**, 51 (2002).
[15] S. Will *et al.* Nature **465**, 197 (2010).
[16] P. R. Johnson, E. Tiesinga, J. V. Porto, and C. J. Williams, N. J. Phys. **11**, 093022 (2009).
[17] A. Smerzi, S. Fantoni, S. Giovanazzi, and R. S. Shenoy, Phys. Rev. Lett. **79**, 4950 (1997).
[18] D. Jaksch, C. Bruder, J. I. Cirac, C. W. Gardiner, and P. Zoller, Phys. Rev. Lett. **81**, 3108 (1998).
[19] C. Orzel *et al.*, Science **291**, 2386 (2001).
[20] A. Widera *et al.*, Phys. Rev. Lett. **100**, 140401 (2008).
[21] S. Fölling *et al.*, Nature **448**, 1029 (2007).
[22] D. Cohen and R. Kottos, Phys. Rev. E **63**, 36203 (2001).
[23] M. Rigol, V. Dunjko, and M. Olshanii, Nature **452**, 854 (2008).